Face Recognition under Makeup

Peixi Xiong (pxx2175)
Northwestern University

Electrical Engineering & Computer Science
peixixiong2018@u.northwestern.edu

1 Abstract

With the development of makeup industry and transform upon aesthetics, people, especially females tend to wear makeup on most occasions. As one of the most common person identity approach, face recognition is required to upgrade with higher accuracy under such circumstance. This project focus on face recognition under makeup and implemented by Dual-Tree Complex Wavelet Transform combined with Local Binary Pattern to extract the features, and setting them as feature vector, then Support Vector Machine is used for classification. The accuracy, ROC curve and CMC curve are shown in the conclusion part.

Keywords: Dual-Tree Complex Wavelet Transform, Local Binary Pattern, DTCWT, LBP

Table of Contents

1 Abstract 2

2 Flowchart 4

3 Method 5

3.1 Dual-Tree Complex Wavelet Transform (DTCWT) 5

3.1.1 Drawback of Traditional Real Wavelets 5

3.1.2 Complex Wavelets 6

3.1.3 Dual-Tree CWT 7

3.1.4 2-D Dual-Tree CWT 8

3.2 Local Binary Pattern (LBP) & Feature Vector 11

3.3 Support Vector Machine 11

4 Results 11

4.1 Recognition Rate on the VMU Database for Several Methods 11

4.2 ROC and CMC 11

5 Conclusion 12

6 Discussion 12

7 References 13

Face Recognition under Makeup

2 Flowchart

Three main steps are implemented in this project, which are shown as follow figure.

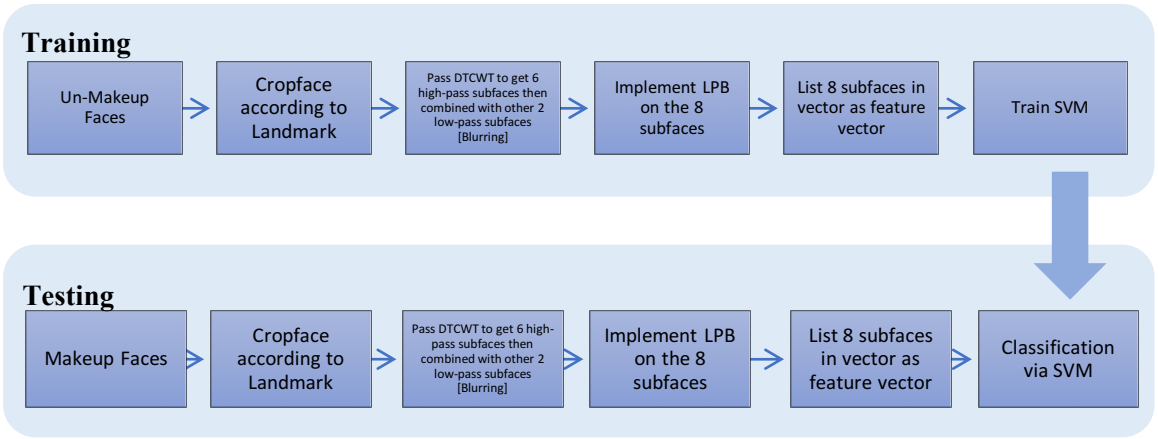

3 Method

3.1 Dual-Tree Complex Wavelet Transform (DTCWT)

The dual-tree complex wavelet transform is a relatively recent enhancement to the discrete wavelet transform. It preserves additional properties that it is nearly shift invariant and directionally selective in two and higher dimensions. [1]

3.1.1 Drawback of Traditional Real Wavelets

3.1.1.1 Oscillations

For the traditional real wavelets, the wavelet coefficient tends to oscillate positive and negative around singularity points. [Figure 1-1] [1]. Such oscillation leads to complication in wavelet-based processing. Besides, since the oscillate function often passes zero, the conventional wisdom that the singularities yield large wavelet coefficients is overstated.

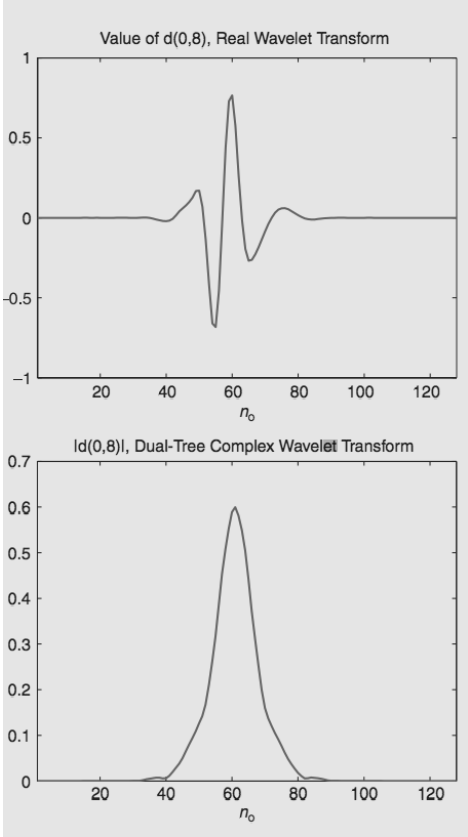

Figure 3-1 Here, the test signal is a step edge at n = n0, x(n) = u(n-n0)

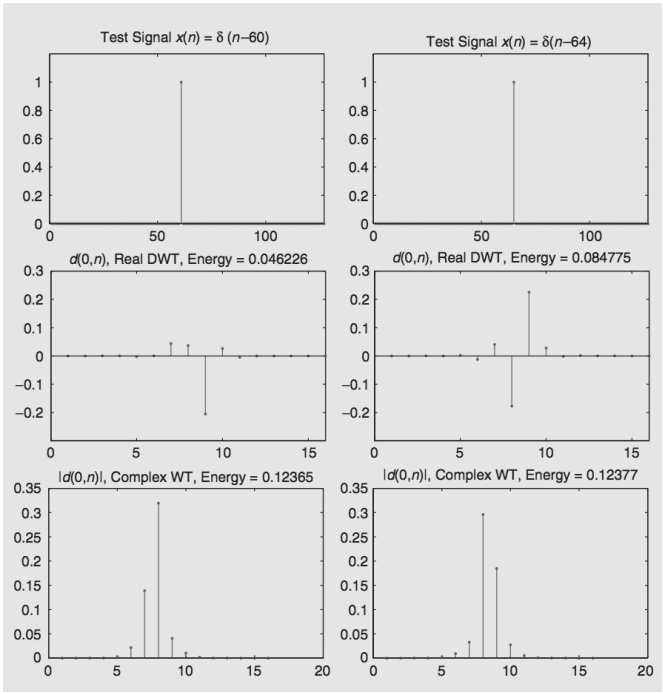

Figure 3-2 The wavelet coefficients of a signal x(n) are very sensitive to translations of the signal.

3.1.1.2 Shift Variance

Besides, the real wavelet is not shift variance, which means that a small shift of the signal leads to great perturbs in the wavelet coefficient around singularity point. [Figure 1-2]. Thus, wavelet-domain processing will be complicated duo to this property.

3.1.1.3 Aliasing

The wide spacing of wavelet coefficient samples are computed via iterated discrete-time down sampling interspersed with no ideal low-pass and high pass filters. [Equation 1]

$$x(t) = \sum_{n=-\infty}^{\infty} c(n)\,\phi(t-n) + \sum_{j=0}^{\infty}\sum_{n=-\infty}^{\infty} d(j,n)\,2^{j/2}\,\psi(2^j t-n).$$

Equation 1 Any finite energy analogue signal x(t) can be decomposed in terms of wavelets and scaling functions, while ∅(t) is a real-valued low-pass scaling function and ψ(t) is a real valued band-pass wavelet.

$$c(n) = \int_{-\infty}^{\infty} x(t)\,\phi(t-n)\,dt,$$

$$d(j,n) = 2^{j/2}\int_{-\infty}^{\infty} x(t)\,\psi(2^j t-n)\,dt.$$

Equation 1 c(n) represents the scaling coefficient and d(j, n) is the wavelet coefficient.

3.1.1.4 Lack of Directionality

Commonly, DWT is implement separately in columns or rows (or other directions), which emphasized the information in some specific direction and weaken others, these leads to the drawback for extraction of the integral image information. In other words, the standard tensor product construction of M-D wavelets produces a checkerboard pattern that is simultaneously oriented along serval directions. The lack of directional selectivity makes processing of image ridges and edges features complicated.

3.1.2 Complex Wavelets

To solve the previous problem and inspired by the Fourier representation, a CWT but with a complex-valued scaling function and complex-valued wavelet is rewritten as Equation 3.

$$\psi_c(t) = \psi_r(t) + j\,\psi_i(t).$$

Equation 2

Here, $\psi_r(t)$ is real and even, while $j\psi_i(t)$ is imaginary and odd. The complex scaling function is defined similarly as shown in Equation 3.

$$\emptyset_c(t) = \emptyset_r(t) + j\emptyset_i(t)$$

Equation 3

Figure 2-3 demonstrates the complex wavelet pair is able to satisfy the properties.

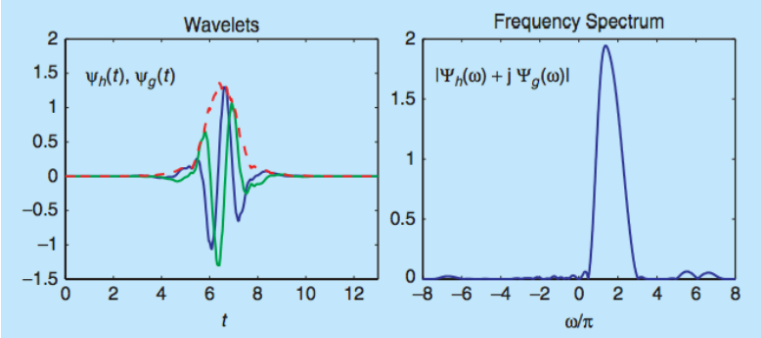

Figure 3-3 A q-shift complex wavelet corresponding to a set of orthonormal dual-tree filters of length 14 [2]

With the projection of signal onto $2^{\frac{j}{2}}\psi_c(2^j t - n)$ as in Equation 1,the complex wavelet coefficient is shown as following. [Equation 4]

$$d_c(j,n) = d_r(j,n) + j\,d_i(j,n) \quad \textit{Equation 4}$$

CWT enables new coherent multiscale signal processing algorithms that exploit the complex magnitude and phase. In particular, a large magnitude indicates the presence of a singularity while the phase indicates its position within the support of the wavelet. [3][4][5][6]

3.1.3 Dual-Tree CWT

With the previous statement, the dual-tree wavelet design is the joint design of filter band (FB) trees to yield a complex wavelet and scaling functions that are as close as possible to analytics. [7][8]

As a result, the DTCWT will yield a smooth, no oscillation magnitude [Refer Figure 1-1]; a nearly shift-invariant magnitude; substantially reduced aliasing; and directional wavelets in higher dimension.

The only cost of DTCWT is the moderate redundancy: 2^d for d-dimensional signals, general. However, it is much less than the $log_2 N\times$ redundancy of a perfectly shift-invariant DWT. [9] [10]

Figure 2-4 demonstrates the structure clearly.

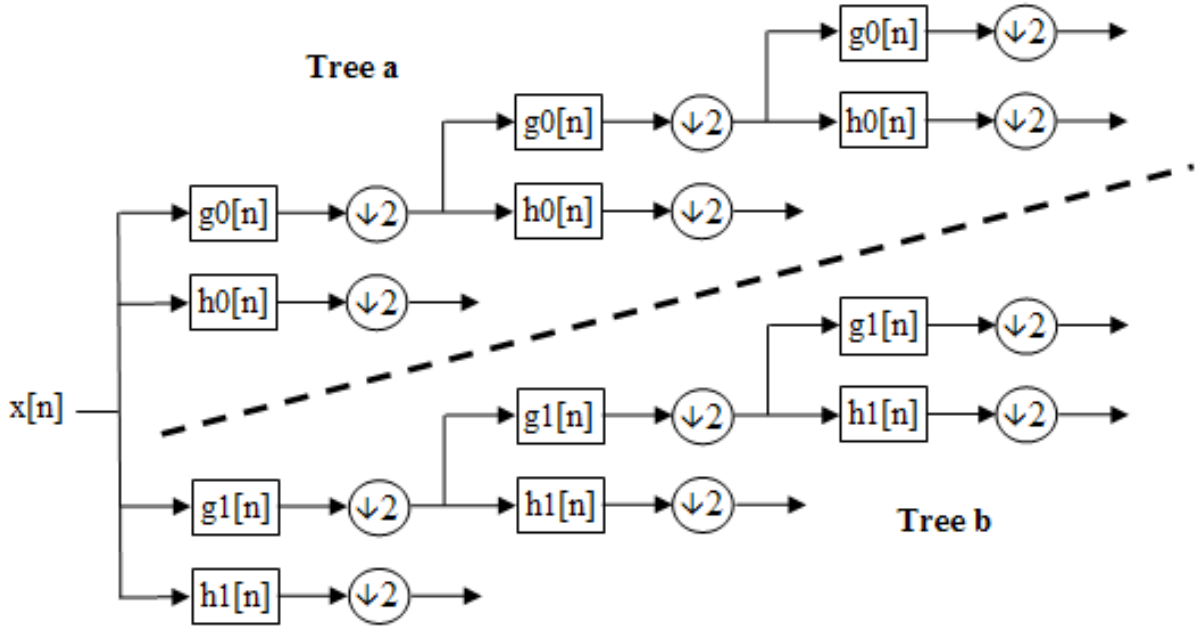

Figure 3-4 Block diagram for a 3 level DTCWT

Let $h0(n), h1(n)$ denote the low-pass/high pass filter pair for the upper filter band, and let $g0(n), g1(n)$ denote the low/high pass filter pair for the lower filter band.

The design of the filters is particularly important for the transform to occur correctly and the necessary characteristics are: [1]

- The low-pass filters in the two trees must differ by half a sample period
- Reconstruction filters are the reverse of analysis
- All filters from the same orthonormal set
- Tree a filters are the reverse of tree b filters
- Both trees have the same frequency response

3.1.4 2-D Dual-Tree CWT

The multidimensional(M-D) dual-tree CWT not only maintains the attractive properties of the 1-D dual-tree, but also obtains additional properties that make it particularly effective for M-D dual-tree wavelet-based signal processing.

Moreover, it is oriented and better for analysing and processing oriented singularities such as edges and ridges in image.

To illustrate how the dual-tree CWT products oriented wavelets, first consider the 2-D wavelet, $\psi(x,y) = \psi(x)\psi(y)$ which is associated with the row-column implementation of the wavelet transform. Here $\psi(x)$ is a complex wavelet given by $\psi(x) = \psi_h(x) + j\psi_g(x)$, according to Figure 2-4.

$$\begin{aligned}\psi(x,y) &= [\psi_h(x) + \mathrm{j}\,\psi_g(x)]\,[\psi_h(y) + \mathrm{j}\,\psi_g(y)] \\ &= \psi_h(x)\,\psi_h(y) - \psi_g(x)\,\psi_g(y) \\ &\quad + \mathrm{j}\,[\psi_g(x)\,\psi_h(y) + \psi_h(x)\,\psi_g(y)].\end{aligned}$$

The support of the Fourier spectrum of this complex wavelet is illustrated by the following idealized diagram. [Figure 2-5]

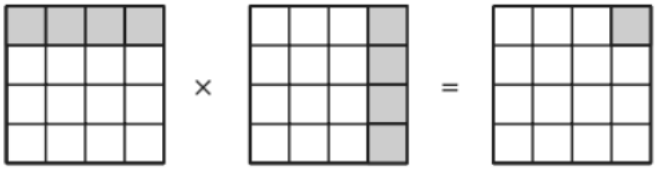

Figure 3-5

For the real part of the complex wavelet, it is the sum of two separable wavelets.

$$\text{Real Part}\{\psi(x,y)\} = \psi_h(x)\,\psi_h(y) - \psi_g(x)\,\psi_g(y).$$

Equation 5

Since the spectrum of a real function must be symmetric with respect to the origin, the spectrum of this real wavelet is supported in two quadrants of the 2-D frequency plane, which is illustrated in figure 2-6. It is obvious that it is oriented at -45°.

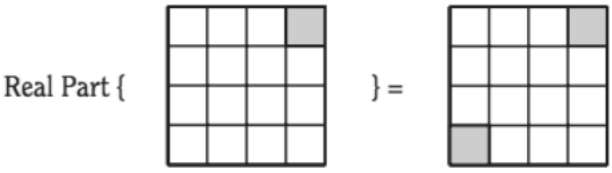

Here, for the first term in Equation 5, $\psi_h(x)\,\psi_h(y)$ are HH wavelet of a separable 2-D real wavelet transform by using filters {h0(n), h1(n)}. Also, the second term $\psi_g(x)\,\psi_g(y)$ is also HH wavelet of a real separable wavelet transform, but uses {g0(n), g1(n)}.

---

*The **LH** wavelet is the product of the **low-pass** function $\varphi(\cdot)$ along the first dimension and the **high-pass** (actually a bandpass) function $\psi(\cdot)$ along the second dimension. The HL and HH wavelets are similarly labelled. While the LH and HL wavelets are oriented vertically and horizontally, the HH wavelet has a checkerboard appearance—it mixes +45° and −45° orientations*

For the +45° wavelet, now choosing $\psi_2(x) = \psi(x)\overline{\psi(y)}$, where $\overline{\psi(y)}$ is the complex conjugate of $\psi(y)$, where $\psi(y) = \psi_h(y) + j\psi_g(y)$. Thus, $\psi_2(x)$ can be rewritten as following.

$$\begin{aligned}\psi_2(x,y) &= [\psi_h(x) + \mathrm{j}\,\psi_g(x)]\,\overline{[\psi_h(y) + \mathrm{j}\,\psi_g(y)]} \\ &= [\psi_h(x) + \mathrm{j}\,\psi_g(x)]\,[\psi_h(y) - \mathrm{j}\,\psi_g(y)] \\ &= \psi_h(x)\,\psi_h(y) + \psi_g(x)\,\psi_g(y) \\ &\quad + \mathrm{j}\,[\psi_g(x)\,\psi_h(y) - \psi_h(x)\,\psi_g(y)].\end{aligned}$$

And the 2-d frequency plane is shown in Figure 2-6.

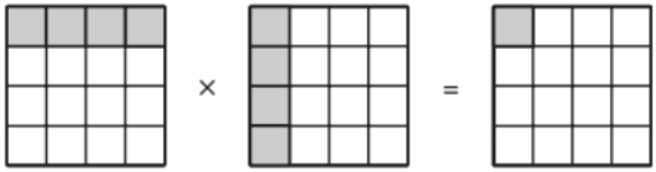

Figure 3-6

The real part of the complex wavelet.

$$\text{Real Part}\{\psi_2(x,y)\} = \psi_h(x)\,\psi_h(y) + \psi_g(x)\,\psi_g(y),$$

The spectrum of this real wavelet.

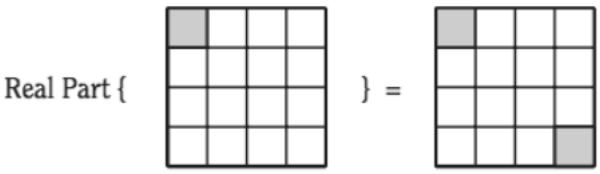

To obtain four more oriented real 2-D wavelets, we can repeat this procedure on the following complex 2-D wavelets: $\emptyset(x)\psi(y)$, $\psi(x)\emptyset(y)$, $\emptyset(x)\overline{\psi(y)}$, and $\psi(x)\overline{\emptyset(y)}$, where $\psi(x) = \psi_h(x) + j\psi_g(x)$ and $\emptyset(y) = \emptyset_h(y) + j\emptyset_g(y)$.

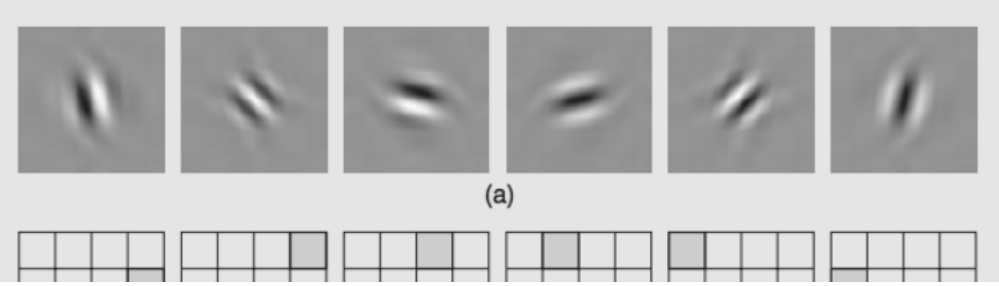

Figure 3-7 Typical wavelets associated with the real oriented 2-D dual-tree wavelet transform. (a) illustrates the wavelets in the space domain; (b) illustrates the (idealized) support of the Fourier

After DTCWT, 6 surfaces are generated, combined with other 2 low-pass image (blurring) to show the general information, 8 surfaces are gotten.

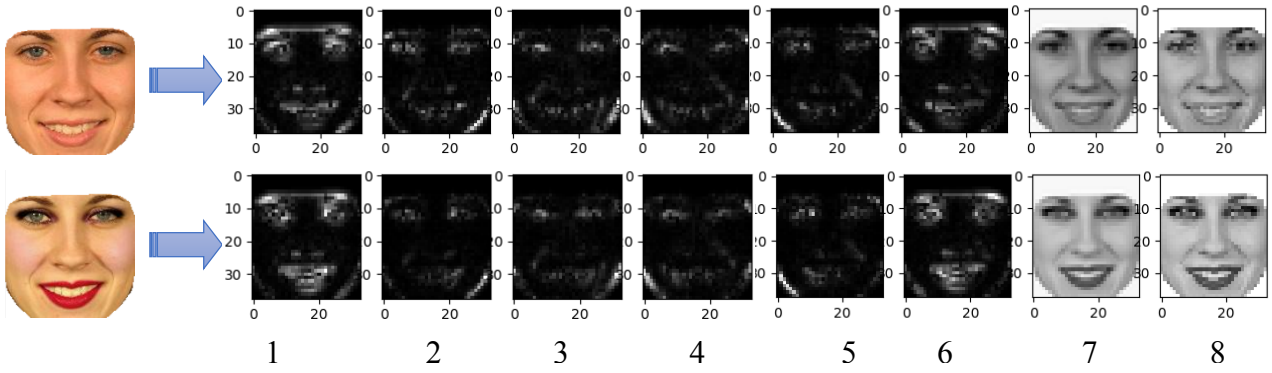

3.2 Local Binary Pattern (LBP) & Feature Vector

Implement the 8 surfaces with LBP and putting them in the feature vector.

feature vector = [1 2 3 4 5 6 7 8]

3.3 Support Vector Machine

One vs rest of SVM classifier with rbf kernel is used here to classify the feature vectors.
Notes: PCA is recommended to use for reducing dimension if the size of feature vector required.

4 Results

4.1 Recognition Rate on the VMU Database for Several Methods

The DTCWT+LBP method was tested on the VMU database[11] [12] [13]. There are 51 female Caucasian synthetically added with makeup in the FRGC database. There are three sets of virtual makeovers. (A) Application only with lips. (B) Application only with eyes (C) Application with full makeup

Two non-makeup images are used for training, while post-makeup images for different area are used separately for testing.

METHOND	TEST SET (A)	TEST SET (B)	TEST SET(C)	MEAN
DTCWT+LBP	96.07%	98.03%	94.11%	96.07%
PCA	90.20%	88.24%	86.28%	88.37%
HOG	82.35%	80.39%	76.47%	79.74%

4.2 ROC and CMC

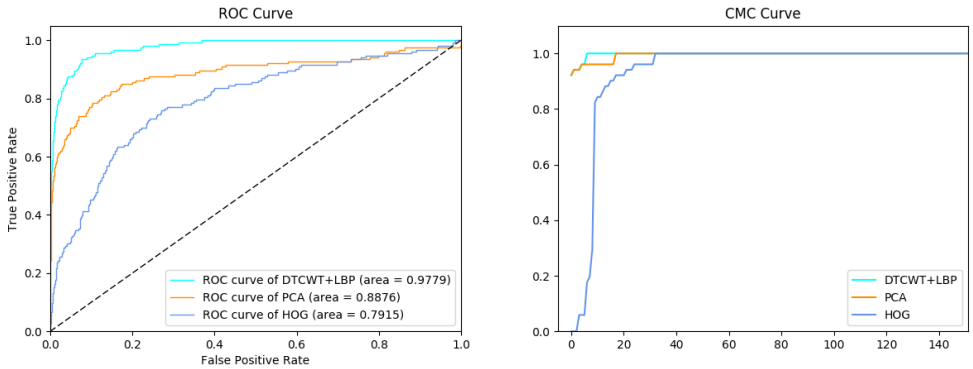

Here is the ROC and CMC curve for all makeup images as test.

5 Conclusion

In this report, the DTCWT with LBP is used for feature extraction and Support Vector Machine. The method is tested on the VMU dataset and the recognition rate, ROC curve and CMC curve are shown as above for demonstration the performance.

6 Discussion

The good performance may be contributed by the invariance posture and face expression. For the real life face recognition under makeup, the illumination, posture, face expression and camera viewpoint need to be considered carefully.

To inprove the algorthm, the relevant parameter in LBP and rbf kernal can be adjusted.
Also, it would be better if tests about changing the filter of the low-pass images in the step three.
Few more state-of-art algrithm upon face recognition should be added as comparision.

7 References

[1]. Selesnick, Ivan W.; Baraniuk, Richard G.; Kingsbury, Nick G. (November 2005). "The Dual-Tree Complex Wavelet Transform"
(PDF). IEEE Signal Processing Magazine. 22 (6): 123–151. doi:10.1109/MSP.2005.1550194.
[2]. N.G. Kingsbury, "Design of q-shift complex wavelets for image processing using frequency domain energy minimization," in Proc. IEEE Int. Conf. Image Processing, Barcelona, Sept. 2003, vol. 1, pp. 1013–1016.
[3]. J. Romberg, M. Wakin, H. Choi, and R.G. Baraniuk, "A geometric hidden Markov tree wavelet model," in Proc. Wavelet Applications Signal Image Processing X (SPIE 5207), San Diego, 2003, pp. 80–86
[4]. J.K. Romberg, M. Wakin, H. Choi, N.G. Kingsbury, and R.G. Baraniuk, "A hidden Markov tree model for the complex wavelet transform," Rice ECE, Tech. Rep., Sept. 2002.
[5]. M. Wakin, "Image compression using multiscale geometric edge models," Master's thesis, Rice Univ., Houston, TX, 2002.
[6]. Z. Wang and E.P. Simoncelli, "Local phase coherence and the perception of blur," in Adv. Neural Information Processing Systems, S. Thrun, L. Saul, and B. Schölkopf, Eds. Cambridge, MA: MIT Press, May 2004, vol. 16.
[7]. N.G. Kingsbury, "Image processing with complex wavelets," Philos. Trans. R. Soc. London A, Math. Phys. Sci., vol. 357, no. 1760, pp. 2543–2560, Sept. 1999.
[8]. N.G. Kingsbury, "Complex wavelets for shift invariant analysis and filtering of signals," Appl. Comput. Harmon. Anal., vol. 10, no. 3, pp. 234–253, May 2001.
[9]. H. Choi, J. Romberg, R.G. Baraniuk, and N. Kingsbury, "Hidden Markov tree modeling of complex wavelet transforms," in Proc. IEEE Int. Conf. Acoust., Speech, Signal Processing (ICASSP), June 5–9, 2000, vol. 1, pp. 133–136.
[10]. M. Lang, H. Guo, J.E. Odegard, C.S. Burrus, and R.O. Wells, Jr., "Noise reduction using an undecimated discrete wavelet transform," IEEE Signal Processing Lett., vol. 3, no. 1, pp. 10–12, Jan. 1996.
[11]. A. Dantcheva, C. Chen, A. Ross, "Can Facial Cosmetics Affect the Matching Accuracy of Face Recognition Systems?," Proc. of 5th IEEE International Conference on Biometrics: Theory, Applications and Systems (BTAS), (Washington DC, USA), September 2012.
[12]. C. Chen, A. Dantcheva, A. Ross, "Automatic Facial Makeup Detection with Application in Face Recognition," Proc. of 6th IAPR International Conference on Biometrics (ICB), (Madrid, Spain), June 2013.
[13]. C. Chen, A. Dantcheva, A. Ross, "An Ensemble of Patch-based Subspaces for Makeup-Robust Face Recognition," Information Fusion Journal, Vol. 32, pp. 80 - 92, November 2016.